

LOW RANK RECOVERY WITH MANIFOLD SMOOTHNESS PRIOR: THEORY AND APPLICATION TO ACCELERATED DYNAMIC MRI

Sunrita Poddar, Mathews Jacob

Department of Electrical and Computer Engineering
The University of Iowa, IA, USA

ABSTRACT

We introduce a regularized optimization algorithm to jointly recover signals that live on a low dimensional smooth manifold. The regularization penalty is the nuclear norm of the gradients of the signals on the manifold. We use this algorithm to reconstruct free breathing dynamic cardiac CINE MRI data. A novel acquisition scheme was used to facilitate the estimation of the manifold structure and recover high quality images. The results show that the method is an efficient alternative to traditional breath-held CINE exams.

Index Terms— free breathing, manifold, low rank, MR image reconstruction, CINE

1. INTRODUCTION

The recovery of dynamic MRI data from undersampled measurements using low rank priors to exploit the high correlation between image frames has witnessed considerable research. These methods perform well in breath-held applications, but the performance degrades with respiratory motion since a model with considerably higher rank is required to reliably approximate the more complex dynamic variations.

We model the images in a dynamic dataset as points on a smooth low-dimensional manifold. Each image in a free breathing dynamic cardiac dataset is a non-linear function of two parameters: cardiac phase and respiratory phase. Hence, these images can be modelled as points on a smooth low-dimensional manifold. Note that the dimension of the manifold is considerably lower than the ambient dimension (number of pixels in the image). We had recently introduced a scheme exploiting manifold smoothness to recover free breathing dynamic datasets [1]. We penalized the sum of squares of ℓ_2 norms of the gradients on the manifold. Since the neighbours of a particular image on the manifold may be well separated in time, this approach is equivalent to non-local smoothing. While this approach gave encouraging results, a limitation was the high memory demand of the algorithm with increasing number of image frames. This

is clearly a drawback since the accuracy of the results can considerably improve with larger number of neighbours.

In this work, we propose to combine the manifold smoothness prior with the low-rank structure of the signal. We penalize the nuclear norm of the gradients of the signals on the manifold, specified by $\mathbf{X}\mathbf{Q}$, where $\mathbf{X} = [\mathbf{x}_1, \mathbf{x}_2, \dots, \mathbf{x}_n]$ is the Casorati matrix of the data and \mathbf{Q} is a gradient operator on the manifold. This encourages low-rank solutions on a smooth manifold. Note that the gradient vectors are free of the mean of the neighbourhoods. Hence this approach may be viewed as modelling the manifold by a union of affine subspaces. We show that the proposed convex penalty can be efficiently solved using a factorization $\mathbf{X} = \mathbf{U}\mathbf{V}$ and an alternating minimization strategy. The factorization provides a significant reduction in memory and computational demands over our previous scheme. This enables us increase the number of frames and obtain significantly improved reconstructions.

We test the proposed algorithm on highly undersampled free breathing CINE data. The manifold structure was estimated from radial navigator signals, acquired using a novel pulse sequence. This approach gave improved results over our earlier approach of estimating the manifold structure from the images (which led to temporal blurring). The results demonstrate the improvement offered by this scheme over classical methods such as low-rank regularization. Our approach has conceptual similarities to [2], where the respiratory and cardiac phase information are estimated using manifold embedding. The data from end expiration was used to recover a CINE movie of the heart with few phases. In contrast, we seek to recover the entire free-breathing dataset without directly estimating the cardiac and respiratory phases. This approach can provide valuable information such as variation of ejection fraction and stroke volume over different heart beats (rather than obtaining an average measure) which could be useful in subjects with arrhythmia.

2. PROBLEM FORMULATION

2.1. Background

We considered the joint recovery of signals $\mathbf{x}_1, \mathbf{x}_2, \dots, \mathbf{x}_k \in \mathcal{M} \subseteq \mathbf{R}^N$ (where \mathcal{M} is a smooth m -dimensional manifold,

This work is supported by CCF-1116067, NIH 1R21HL109710-01A1, ACS RSG-11-267-01-CCE and ONR grant N00014-13-1-0202.

$m \ll N$), from its under sampled measurements [1]:

$$\mathbf{b}_i = \mathbf{A}_i \mathbf{x}_i + \boldsymbol{\eta}_i. \quad (1)$$

Here, $\mathbf{A}_i \in \mathbb{C}^{M \times N}$; $M < N$ is the measurement operator and $\boldsymbol{\eta}_i$ is the noise vector for the i^{th} frame. The smoothness of the underlying manifold was exploited by posing the recovery as the following discretized Tikhonov regularized reconstruction scheme:

$$\{\mathbf{x}_i^*\} = \arg \min_{\mathbf{x}_i} \sum_{i=1}^k \|\mathbf{A}_i \mathbf{x}_i - \mathbf{b}_i\|_F^2 + \lambda \text{Tr}(\mathbf{X} \mathbf{L} \mathbf{X}^H) \quad (2)$$

where $\mathbf{X} = [\mathbf{x}_1 \ \mathbf{x}_2 \ \dots \ \mathbf{x}_k]$ and \mathbf{L} is the Laplacian of the associated graph. Since the graph Laplacian can be factorized as $\mathbf{L} = \mathbf{Q} \mathbf{Q}^T$, the recovery problem (2) can be rewritten as:

$$\{\mathbf{x}_i^*\} = \arg \min_{\mathbf{x}_i} \sum_{i=1}^k \|\mathbf{A}_i \mathbf{x}_i - \mathbf{b}_i\|_F^2 + \lambda \|\mathbf{X} \mathbf{Q}\|_F^2. \quad (3)$$

We term \mathbf{Q} as the gradient operator on the manifold. For $k = 4$, \mathbf{Q} is given by :

$$\mathbf{Q}^T = \begin{bmatrix} \sqrt{\mathbf{w}_{12}} & -\sqrt{\mathbf{w}_{12}} & 0 & 0 \\ 0 & \sqrt{\mathbf{w}_{23}} & -\sqrt{\mathbf{w}_{23}} & 0 \\ 0 & 0 & \sqrt{\mathbf{w}_{34}} & -\sqrt{\mathbf{w}_{34}} \\ \sqrt{\mathbf{w}_{13}} & 0 & -\sqrt{\mathbf{w}_{13}} & 0 \\ 0 & \sqrt{\mathbf{w}_{24}} & 0 & -\sqrt{\mathbf{w}_{24}} \\ \sqrt{\mathbf{w}_{14}} & 0 & 0 & -\sqrt{\mathbf{w}_{14}} \end{bmatrix} \quad (4)$$

Here \mathbf{w}_{ij} is the $(i, j)^{\text{th}}$ element of the weight matrix \mathbf{W} of the associated graph. The method for computation of the weights is explained in section 2.2.

Our experiments show that increasing the number of frames of \mathbf{X} result in improved recovery. This is not surprising since having a larger dataset ensures that each frame has a larger number of neighbours (frames that are similar to it) which aids recovery. However, the computational complexity and memory demand of the direct minimization of (3) is prohibitively high for large datasets.

2.2. Estimation of the manifold structure

We introduce a novel acquisition scheme to facilitate the estimation of the manifold structure. Specifically, each frame is sampled using a combination of two Fourier sampling operators:

$$\mathbf{A}_i = \begin{bmatrix} \boldsymbol{\Phi} \\ \mathbf{B}_i \end{bmatrix} \quad (5)$$

$\boldsymbol{\Phi}$ acquires k-space data at identical sampling locations in all frames. In contrast, \mathbf{B}_i samples k-space at different locations in each frame. The matrices $\boldsymbol{\Phi}$ and \mathbf{B}_i used in this paper are described in section 2.4. The data acquired by $\boldsymbol{\Phi}$ for a particular frame is termed the navigator signal for that frame. The navigator signal for the i^{th} frame is given by:

$$\mathbf{y}_i = \boldsymbol{\Phi} \mathbf{x}_i \quad (6)$$

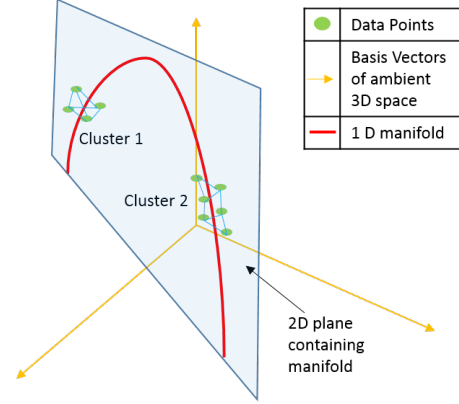


Fig. 1. Two disjoint data clusters are shown lying close to a 1D manifold (in red). The ambient space is 3D, but the 1-D manifold lies on the 2D plane shown in blue. Minimization of the nuclear norm of the manifold gradient $\mathbf{X} \mathbf{Q}$ brings the points in the cluster closer to the curve, while constraining it to the subspace. The proposed scheme is more desirable than simple low rank regularized recovery (which just restricts the reconstructed data points to the 2D plane) or manifold smoothness recovery (which restricts the reconstructed data points to lie near the 1D manifold).

These samples \mathbf{y}_i can be used to compute the weights w_{ij} using any appropriate localized non-linear function. A commonly used function is :

$$w_{i,j} = \begin{cases} e^{-\frac{\|\mathbf{y}_i - \mathbf{y}_j\|^2}{\sigma^2}} & \text{if } \|\mathbf{y}_i - \mathbf{y}_j\|_2^2 < \mathbf{t} \\ 0 & \text{else} \end{cases} \quad (7)$$

where \mathbf{t} is some fixed threshold. A large value of \mathbf{t} results in a densely connected graph with more dissimilar nodes being connected. A smaller value of σ leads to more localized or faster decaying weights. The matrix of weights \mathbf{W} is further denoised using the spectral clustering method by Shi and Malik [3]. This shrinks smaller weights, thus reducing inter-cluster interaction, which results in improved recovery.

2.3. New formulation

In this work, we propose to exploit the low-rank structure of the image gradients on the manifold by considering the following optimization problem:

$$\{\mathbf{X}^*\} = \arg \min_{\mathbf{X}} \|\mathbf{X} \mathbf{Q}\|_* \quad (8)$$

s.t. $\mathbf{A}_i \mathbf{x}_i = \mathbf{b}_i$

The nuclear norm compactness prior encourages the gradients on the manifold to be low-rank. Since the gradient vectors are free of the mean of the manifold neighbourhoods, this approach encourages the approximation of the manifold by a union of affine subspaces. This is more desirable than the classical low-rank approximation, as illustrated in Fig 1.

Assuming the data matrix \mathbf{X} to be low rank, we factorize it as:

$$\mathbf{X} = \mathbf{U} \mathbf{V} \quad (9)$$

where $\mathbf{U} \in \mathbf{R}^{N \times r}$, $\mathbf{V} \in \mathbf{R}^{r \times k}$ and $\text{rank}(\mathbf{X}) = r$. In our case of the cardiac data time series, this is a valid assumption since the images are highly correlated. Here \mathbf{U} corresponds to basis images and \mathbf{V} corresponds to temporal basis functions. The i^{th} column of the matrix \mathbf{V} is given by \mathbf{v}_i . It can be shown (along the lines of [4]) that the following optimization problem:

$$\{\mathbf{U}^*, \mathbf{V}^*\} = \arg \min_{\mathbf{U}, \mathbf{V}} \frac{1}{2} (\|\mathbf{U}\|_F^2 + \|\mathbf{V}\mathbf{Q}^\epsilon\|_F^2) \quad (10)$$

s.t. $\mathbf{A}_i \mathbf{U} \mathbf{v}_i = \mathbf{b}_i$

is equivalent to:

$$\{\mathbf{X}^*\} = \arg \min_{\mathbf{X}} \|\mathbf{X}\mathbf{Q}^\epsilon\|_* \quad (11)$$

s.t. $\mathbf{A}_i \mathbf{x}_i = \mathbf{b}_i$

in the sense that $\mathbf{X}^* = \mathbf{U}^* \mathbf{V}^*$ and both the objective functions of (10) and (11) reach the same minimum value subject to the given constraints. Here, \mathbf{Q}^ϵ is obtained by replacing the zero singular values of \mathbf{Q} with some infinitesimally small value ϵ . If we define $\mathbf{L}^\epsilon = \mathbf{Q}^\epsilon \mathbf{Q}^{\epsilon T}$, then \mathbf{L}^ϵ can be obtained by replacing the zero singular values of the Laplacian \mathbf{L} with ϵ^2 .

In reality, the measurements are corrupted with noise and our goal is to recover the under-sampled signals \mathbf{x}_i by solving the optimization problem:

$$\{\mathbf{U}^*, \mathbf{V}^*\} = \arg \min_{\mathbf{U}, \mathbf{V}} \sum_i \|\mathbf{A}_i \mathbf{U} \mathbf{v}_i - \mathbf{b}_i\|^2 + \lambda (\|\mathbf{U}\|_F^2 + \|\mathbf{V}\mathbf{Q}^\epsilon\|_F^2) \quad (12)$$

and setting $\mathbf{X} = \mathbf{U}^* \mathbf{V}^*$.

We assume that the graph associated with \mathbf{L} has q connected components and \mathcal{C}_p is the set of nodes in the p^{th} connected component where $p = 1, 2, \dots, q$. The objective function in (12) can be rewritten as: $\sum_i \|\mathbf{A}_i \mathbf{U} \mathbf{v}_i - \mathbf{b}_i\|^2 + \lambda (\|\mathbf{U}\|_F^2 + \|\mathbf{V}_1 \mathbf{Q}_1^\epsilon\|_F^2 + \|\mathbf{V}_2 \mathbf{Q}_2^\epsilon\|_F^2 + \dots + \|\mathbf{V}_q \mathbf{Q}_q^\epsilon\|_F^2)$. Here \mathbf{V}_p is a matrix containing the columns of \mathbf{V} corresponding to the indices in \mathcal{C}_p . \mathbf{Q}_p^ϵ can similarly be obtained by choosing the appropriate rows of \mathbf{Q}^ϵ . This can be interpreted as promoting similarity between the temporal profiles of images within the same cluster. Similar temporal profiles within a cluster enforces similarity between images in that cluster thus leading to a low rank of the manifold gradient as desired by (11). This gives some intuition regarding the equivalence between (12) and (11), and our choice of objective function.

Problem (12) is solved by alternating between minimization with respect to \mathbf{U} and \mathbf{V} . This requires an initial guess for the temporal basis matrix \mathbf{V} . For this purpose, we use the samples \mathbf{y}_i from (6) following the ideas in [5]. The initial guess is obtained by performing a singular value decomposition on the matrix \mathbf{Y} and retaining the first n right subspace vectors obtained. Here $\mathbf{Y} = [\mathbf{y}_1 \quad \mathbf{y}_2 \quad \dots \quad \mathbf{y}_k]$ and n is some chosen number such that $n > r$.

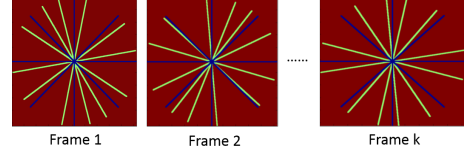


Fig. 2. K-space sampling masks. Blue: Sampling mask for navigator signals (same sampling locations every frame). Green: Sampling mask corresponding to a continuous radial Golden angle acquisition (different sampling locations every frame). Red: Locations of k-space that are not sampled.

Recovery and storage of only \mathbf{U} and \mathbf{V} is more memory efficient than the recovery and storage of \mathbf{X} . In the former case we have to store two matrices of size $N \times n$ and $n \times k$ respectively, whereas in the latter case we have to store one matrix of size $N \times k$. Typically N is large (say 512^2) and n is small (say 50). A large value of k implies a long acquisition time, but a better recovery. For $N = 512^2$, $n = 50$ and $k = 1000$, the low rank decomposition reduces memory usage by almost a factor of 20.

2.4. Application to free breathing cardiac CINE MRI

We developed a novel sampling scheme as described in (5) to facilitate the estimation of the manifold structure and reconstruction, using a modified golden angle radial sampling strategy (Fig 2). In the classical golden angle radial sampling strategy, the angle between consecutively acquired radial lines of k-space is approximately 111.25° . For our modified scheme each image frame is to be reconstructed from p lines of k-space out of which s lines are navigator lines. These s radial lines of k-space are acquired at fixed angles of $\frac{i \times 180^\circ}{s}$ every frame where $i = 0, 1, 2, \dots, s - 1$. The rest of the lines ($p - s$ per frame) are acquired continuously by a classical golden angle trajectory. If $p = 5$ and $s = 2$, the lines numbered 3, 4, 5, 8, 9, 10, 13, 14, 15... are consecutive lines of a classical golden angle acquisition.

The sequence was implemented on a 3T Siemens Trio scanner. The data was acquired using a SSFP sequence with an 18 channel coil array, with TR/TE 4.2/2.1 ms, matrix size 512×512 , FOV 300mm \times 300mm and slice thickness 5mm. In this paper, we used 10 radial lines of k-space to reconstruct each image frame, 4 of which were navigator lines. This translated to a temporal resolution of 42 ms. For factorization according to (9), we considered $n = 50 > r$. The acquisition time was 42 s corresponding to 1000 frames.

3. RESULTS

3.1. Numerical simulations

A short axis view of the PINCAT phantom [6] torso (with both cardiac and respiratory motion) was used to study the effect of the number of common lines on the weight computation. This is illustrated in Fig 3. The matrix size of this dataset was 128×128 and we used a time series containing 500 frames.

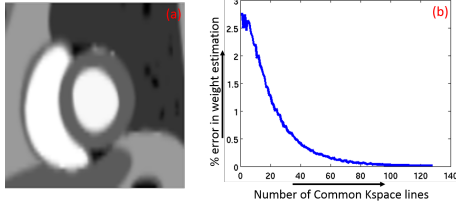


Fig. 3. (a) A single frame of the PINCAT phantom. (b) Plot showing error in computation of weights (according to (7) followed by denoising using spectral clustering) with respect to number of common kspace lines measured.

This corresponds to around 29 cardiac cycles and 6 respiration cycles. A frame of the phantom is shown in Fig 3(a). In Fig 3(b) error in weight computation is plotted against the number of navigator lines per frame. It is observed that around 2% error is incurred when 10 navigator lines are used. Note that for our dataset acquired on the MR scanner, we have an 18 channel coil array, each acquiring 4 navigator lines per frame. This translates to using $18 \times 4 = 72$ navigator lines per frame to estimate the weights.

3.2. Experimental data

The acquired MRI data was reconstructed using the proposed scheme and several state of the art methods. The comparisons are shown in Fig 4. The rows correspond to the reconstructions using (a) nuclear norm minimization, (b) PSF recovery [5], where \mathbf{V} is computed using the SVD of the matrix of common lines \mathbf{Y} and \mathbf{U} is computed using the least squares minimization, (c) PSF recovery with spatial total variation regularization of \mathbf{U} , and (d) the proposed algorithm (12). It is observed that images in (a) exhibit considerable spatial blurring. The PSF scheme in (b), which corresponds to hard thresholding of singular values, provides sharper results. However, there are considerable streaking artifacts. The use of spatial TV regularization in PSF model (c) is observed to blur the features of most images without fully removing the streaking artifacts. The image in column 2 shows sharper features on the application of spatial TV. In (d) the streaking artifacts are eliminated, without considerable edge blurring.

4. CONCLUSION

An algorithm was proposed to recover undersampled data which has a low rank structure and lies on a low dimensional smooth manifold. This algorithm was used to recover a free-breathing cardiac image series from its kspace samples. A novel acquisition scheme was designed to estimate the manifold structure from the kspace data. Good quality and high temporal resolution images were obtained, making the proposed method a simple and efficient alternative to traditional breath-held CINE. The method performs significantly better than low rank methods with and without total variation priors. The quality of the reconstructions may further be improved using spatial total variation regularization.

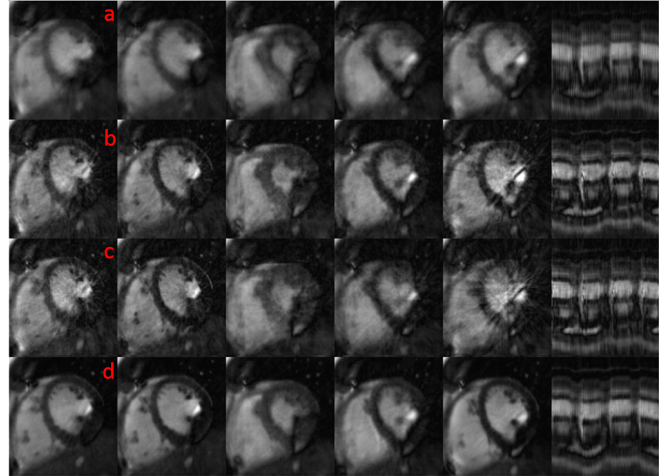


Fig. 4. Reconstructions of free breathing CINE data using different algorithms: The rows correspond to reconstructions obtained using (a) Nuclear Norm minimization recovery (b) Low rank recovery with \mathbf{V} obtained by SVD of \mathbf{Y} (matrix of common kspace lines) and \mathbf{U} recovered using a least squares minimization (c) Similar approach as (b) with addition of spatial TV regularization on \mathbf{U} (d) Recovery using the new algorithm given by (12). The first five columns are representative images from the time series (cropped to include only the myocardium), while the last column shows the temporal intensity profile of the reconstructions along a vertical line.

5. REFERENCES

- [1] S.Poddar, S.Lingala, and M.Jacob, "Joint recovery of undersampled signals on a manifold : Application to free-breathing cardiac MRI," ICASSP, Florence, 2014.
- [2] M.Usman, D.Atkinson, C.Kolbitsch, T.Schaeffter, and C.Prieto, "Manifold learning based ECG-free free-breathing cardiac CINE MRI," *JMRI*, 2014.
- [3] J.Shi and J.Malik, "Normalized cuts and image segmentation," *IEEE Transactions on PAMI*, 2000.
- [4] M.Fazel, *Matrix Rank Minimization with Applications*, Ph.D. thesis, Stanford University, 2002.
- [5] Z.Liang, "Spatiotemporal imaging with partially separable functions," ISBI, Washington DC, 2007.
- [6] B. Sharif and Y. Bresler, "Physiologically improved ncat phantom (pincat) enables in-silico study of the effects of beat-to-beat variability on cardiac MR," Annual Meeting of ISMRM, Berlin, 2007.